Journal of Nuclear Materials 390–391 (2009) 755–759

Contents lists available at ScienceDirect

Journal of Nuclear Materials

journal homepage: www.elsevier.com/locate/jnucmat

The impact of large ELMs on JET

R.A. Pitts [a,b,*], G. Arnoux [a,c], M. Beurskens [c], T. Eich [d], W. Fundamenski [c], A. Huber [e], A. Loarte [f], J. Marki [b], M.F. Stamp [c], P. Andrew [c,1], S. Brezinsek [e], H.G. Esser [e], B. Gulejova [b], S. Jachmich [g], A. Kreter [e], E. de la Luna [f], G.F. Matthews [c], V. Philipps [e], E. Solano [h], JET EFDA Contributors [2]

[a] JET-EFDA Culham Science Centre, Abingdon OX14 3DB, UK
[b] CRPP-EPFL, Association EURATOM-Confédération Suisse, CH-1015 Lausanne, Switzerland
[c] Euratom/UKAEA Fusion Association, Culham Science Centre, Abingdon OX14 3DB, UK
[d] Max-Planck-Institut für Plasmaphysik, IPP-EURATOM Association, D-85748 Garching, Germany
[e] Institut für Energieforschung-Plasmaphysik, Forschungszentrum Jülich, Association EURATOM-FZJ, Germany
[f] ITER Organization, CEA-Cadarache Centre, 13108 Saint Paul les Durance, France
[g] LPP, ERM/KMS, Association Euratom-Belgian State, B-1000 Brussels, Belgium
[h] Associacion Euratom/CIEMAT Para Fusion, Madrid, Spain

ARTICLE INFO

PACS:
52.55.−s
52.55.Fa

ABSTRACT

To ensure sufficient divertor target lifetime, the loss in plasma stored energy due to ELMs in ITER should be restricted to $\Delta W_{ELM} \leqslant 1$ MJ. Only in JET, by virtue of its size, can such energies be approached. This contribution examines the impact of large, Type I ELMs in high current H-mode JET discharges with ITER-relevant pedestal characteristics. The ELMs provoke strong radiation losses, mostly confined to the inner divertor volume. Although the data are scattered, the average magnitude of this loss is $\Delta E_{RAD} \sim 0.5\Delta W_{ELM}$, for $\Delta W_{ELM} < 0.55$ MJ. For higher ΔW_{ELM}, greater fractional radiation losses occur, reaching $\sim 0.7\Delta W_{ELM}$ at $\Delta W_{ELM} \sim 0.9$ MJ, indicating enhanced impurity release. Even at the highest ELM energies, peak divertor target surface temperatures are too low for carbon sublimation, suggesting that thermal decomposition and/or ablation of thick co-deposited layers on the inner target may be occurring. On average, across the range of energies studied, ELMs are found to deposit between 3–4.5% of ΔW_{ELM} on main wall limiters. When applied to the data for a specific discharge in the series, the model of ELM filament parallel energy losses developed at JET requires radial ELM velocities in the interval 0.1–0.65 km s^{-1} to explain these deposited energy fractions.

1. Introduction

Recent materials research has shown that in order to prevent unacceptable divertor target erosion due to edge localised mode (ELM) transient heat loads in ITER, the energy flux at divertor or first wall surfaces should not exceed ~0.5 MJ m^{-2}, corresponding to a loss in plasma stored energy at the ELM of $\Delta W_{ELM} \sim 1$ MJ [1]. For the projected ITER $Q_{DT} = 10$ baseline scenario this implies $\Delta W_{ELM}/W_{plasma} \sim 0.003$, smaller than any value currently found experimentally for (unmitigated) Type I ELMs. It is, however, considerably larger than can be accessed by today's devices, with the exception of JET which, by virtue of its size, can produce ELMs close to 1 MJ. This contribution summarises the results of experiments at JET designed to study large ELMs and to characterise their impact on the divertor plasma and on first wall and divertor target surfaces.

2. Experiment

To access the highest possible ΔW_{ELM}, JET has been run at $I_p = 3.0$ MA ($B_\varphi = 3.0$ T, $q_{95} \sim 3.1$) in a series of dedicated discharges with fixed plasma shape ($\delta = 0.25$, $\kappa = 1.72$), progressively decreasing the gas fuelling, Γ_{gas}, from shot to shot. This produces a scan in ELM amplitude and frequency at high W_{plasma} (~8 MJ) with the largest $\Delta W_{ELM} \sim 0.8$–0.9 MJ being found at $\Gamma_{gas} = 0$, for which the plasma density reaches only ~0.4 of the Greenwald limit. The plasma shape in this recent experiment is very close to the diagnostic optimised configuration (DOC-L) used in the past for ELM studies on JET [2] and is a vertical target equilibrium with strike points on the lower, CFC vertical tiles of the MarkII HD divertor (Fig. 1). Tiles 3 and 7 are unique amongst the target set in having one of

* Corresponding author. Present address: ITER Organization, CS 90 046, 13067 St. Paul-lez-Durance cedex, France.
E-mail address: richard.pitts@iter.org (R.A. Pitts).
[1] Present address: ITER Organization, CS 90 046, 13067 St. Paul-lez-Durance cedex, France.
[2] See the Appendix of M.L. Watkins et al., Fus. Energy, 2006 (Proceedings of the 21st International Conference, Chengdu, 2006) IAEA, 2006.

0022-3115/$ - see front matter © 2009 Elsevier B.V. All rights reserved.
doi:10.1016/j.jnucmat.2009.01.201

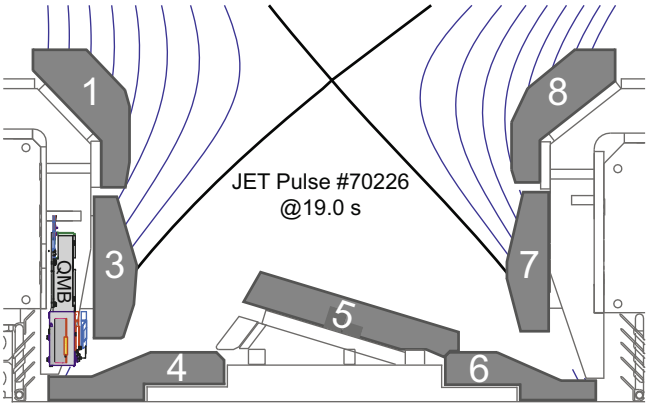

Fig. 1. MarkIIHD divertor configuration with EFIT reconstruction.

the CFC fibre weaves in the toroidal direction, restricting poloidal heat conduction and maximising the surface temperature increase for a given heat load.

A selection of key plasma parameters for one of the recent unfuelled H-modes is compiled in Fig. 2(a)–(g). With a total power input (Fig. 1(b)) of ~20 MW (NBI heating and a small amount of ICRH since coupling efficiency is limited during large ELMs), the injected energy in these discharges is in the range 160–195 MJ. Of this, ~90 MJ is found on Tiles 3 and 7 (Fig. 1) in the ratio 2.9–3.5:1 in favour of the outer target, entirely consistent with earlier findings for ELM averaged energy asymmetries [3]. Total radiated energies in the range 70–90 MJ provide reasonable global power balance across the discharge series. The largest ELMs are generally sporadic (Fig. 2(a)) and often compound, characterised by a sharp initial drop in W_{plasma} and followed by a phase of smaller ELMs (possibly Type III), during which stored energy leaks out on a slower timescale. Energy confinement (expressed in terms of the $H_{98}(y,2)$ scaling (Fig. 2(f)) generally remains above unity, implying that the compound phases do not signal a return to L-mode. In the pre-ELM phases, electron temperature and density at the H-mode pedestal top (Fig. 2(d) and (e)) are in the ranges 5–6 $\times$ 10^{19} m^{-3} and 2–2.5 keV, respectively, yielding neoclassical pedestal collisionalities $\nu_e^* = 0.03–0.06$ expected on ITER [2] and $\Delta W_{ELM}/W_{ped} \sim 0.2$ for the largest ELMs. In general, large ELMs provoke only modest increases in line integral Z_{eff} (Fig. 2(g)), with the exception of isolated events (e.g. prolonged compound phases) during which confinement is degraded significantly.

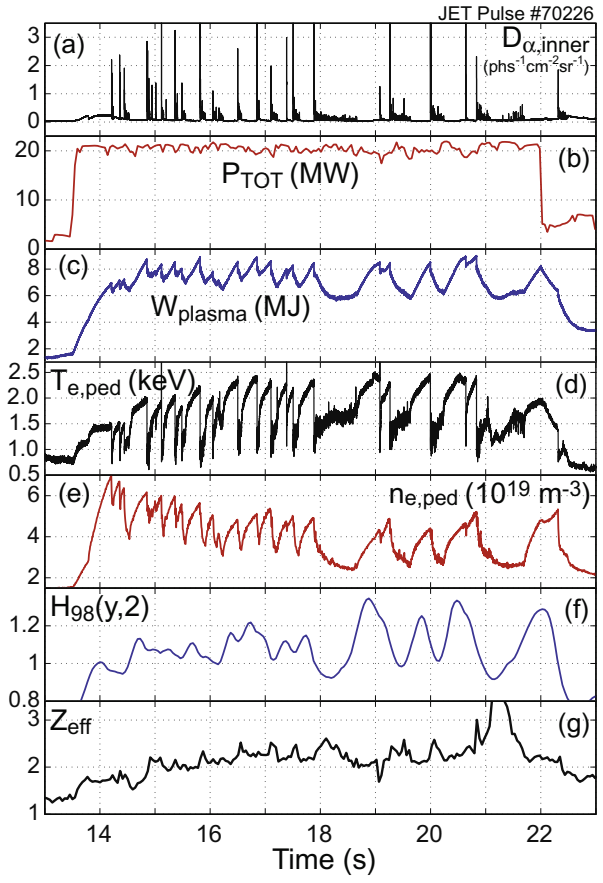

Fig. 2. (a)–(g) Selected plasma signals for a 3.0 MA H-mode discharge with $\Gamma_{gas} = 0$.

3. ELM-induced radiation

Thanks to a major upgrade of the JET bolometer camera diagnostic [4], a 10-fold increase in time resolution compared with the previous system now permits measurement of the energy radiated per ELM on the 1 ms timescale. Fig. 3(a) concentrates on a single large event with $\Delta W_{ELM} \sim 0.85$ MJ, of which $\Delta E_{RAD} = 0.58$ MJ is radiated within ~6 ms of the pedestal crash ($\Delta W_{ELM}/\Delta E_{RAD} = 0.68$). By the end of the compound phase, a total of 1.29 MJ of stored energy has been lost, of which 1.08 MJ (84%) has been radiated. The

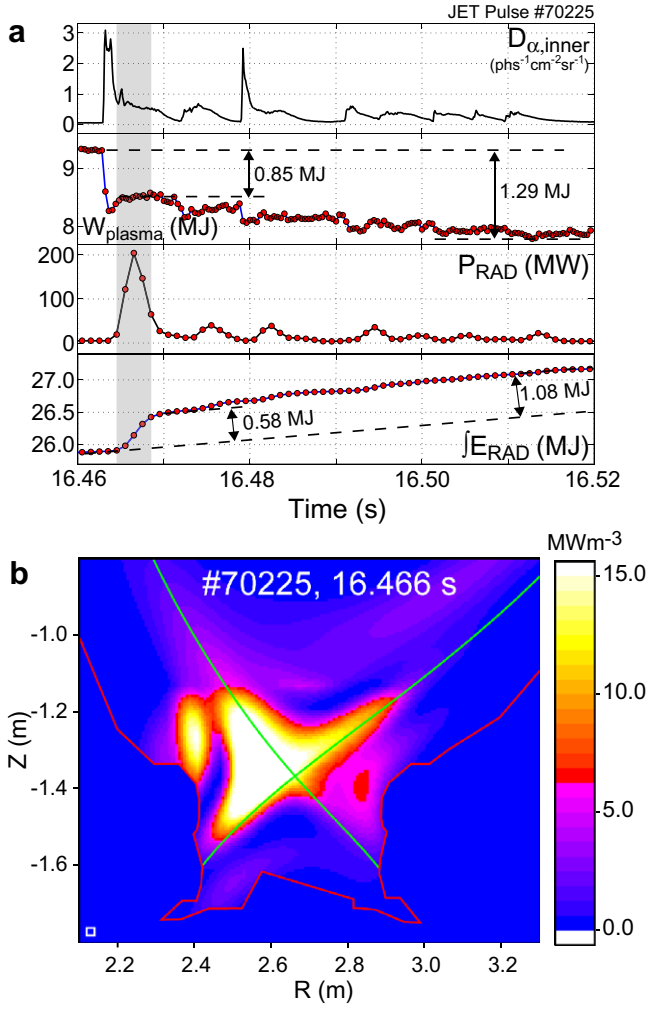

Fig. 3. (a) Energy balance during a single large ELM. (b) Tomographic reconstruction of the ELM radiation distribution averaged over shaded region in (a).

tomographic reconstruction shown in Fig. 3(b), averaged over the ~4 ms period of the main radiated power peak following the ELM crash (inversions on the 1 ms timescale are numerically difficult to produce) illustrates the localisation of the radiated power distribution in the inner divertor volume (similar to ELM resolved bolometric reconstructions first performed on ASDEX Upgrade [5]). This is very likely to be a consequence of two principal factors: (i) the ELMs are known to deposit their energy asymmetrically, very clearly favouring the inner divertor over the outer in the ratio ~2:1 on JET [6] and (ii) the inner divertor is a region of strong net co-deposition, with thick, deuterium rich carbon layers accumulating over any given operational campaign [7].

The single ELM case shown in Fig. 3 is included in Fig. 4 which provides the ΔE_{RAD} dependence on ΔW_{ELM} for all ELMs identified in the 3.0 MA gas scan series (initial ELM crash only). There is clearly considerable scatter in the data, testifying to the fact that individual ELMs of similar energy do not yield the same divertor radiative response. The radiated fractions fall solidly within the envelope 25–100% of ΔW_{ELM} and follow an approximate quadratic trend with ΔW_{ELM} (see dashed lines in Fig. 4). The solid triangular symbols and associated error bars in Fig. 4 are mean values and standard deviations over small intervals of W_{ELM} (7 intervals of ~0.06 MJ up to W_{ELM} = 0.5 MJ and 5 intervals of ~0.08 MJ for 0.5 MJ < ΔW_{ELM} < 0.9 MJ). They illustrate that $\Delta E_{RAD} \sim 0.5\Delta W_{ELM}$ is approximately satisfied up to ΔW_{ELM} = 0.5 MJ, but that for higher values (of which the ELM in Fig. 3 is an example, marked by the star symbol in Fig. 4), there are indications for an enhanced effect (see also [8]).

These ELM-induced radiation losses may be compared with those reported in [9] from the earlier DOC-L experiment in the MarkIISRP divertor (before the bolometer diagnostic upgrade), where $\Delta E_{RAD} \sim 0.25\Delta W_{ELM}$ was observed for $\Delta W_{ELM} \leqslant 0.7$ MJ (similarly to Fig. 4), marking a sharp threshold beyond which radiation was considerably enhanced. In fact, the values of ΔW_{ELM} were somewhat overestimated in [9] (due to perturbations during the ELM affecting the diamagnetic loop measurement which were not recognised at the time) such that the threshold probably occurred even earlier. In the absence of target surface temperature measurements, thermal sublimation was proposed as the mechanism for the apparently increased impurity release. Analysis of IR data obtained during these older experiments (the equivalent data in the more recent experiment is unfortunately lacking) has since become available. It is compiled in Fig. 5, showing the peak surface temperature dependence on ΔW_{ELM} (corrected for dynamic perturbations to the diamagnetic loop signal) for a range of DOC-L discharges with varying I_p (but mostly constant q_{95}), during which the largest $\Delta W_{ELM} \sim 0.7$ MJ were also obtained at I_p = 3.0 MA. The effect of surface layers can be seen in the abrupt rise in temperature on the inner target in response to the ELM, even at low ΔW_{ELM}. Maximum ELM driven excursions of ~520 °C and ~550 °C are seen at the outer and inner targets respectively, pushing temperatures up to ~1130 °C at the outer (where the higher inter-ELM heat fluxes drive the baseline temperature higher). Even though instrumental considerations could imply that the real temperature is somewhat higher, this correction is unlikely to exceed ~200 °C, so that the peak values cited above are still far short of what is required for radiation enhanced sublimation of graphite, which becomes effective in the region of 2200 °C and above in tokamaks [10].

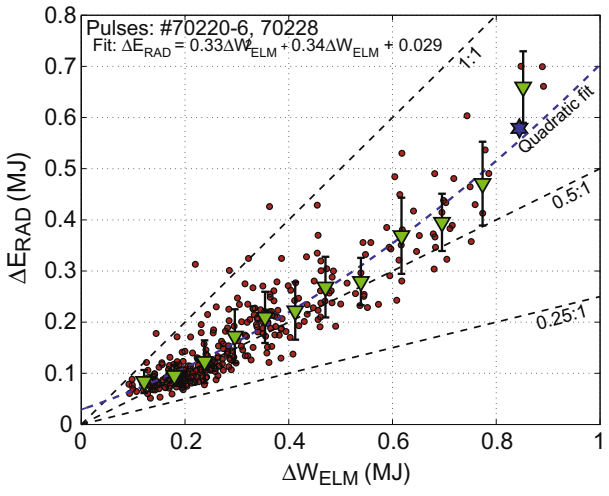

Fig. 4. ΔE_{RAD} at the ELM crash vs. ΔW_{ELM} for all ELMs found in the 3.0 MA shot series. The ▼ are mean values of the data over short intervals in ΔW_{ELM}. The ✱ symbol marks the ELM examined in detail in Fig. 2.

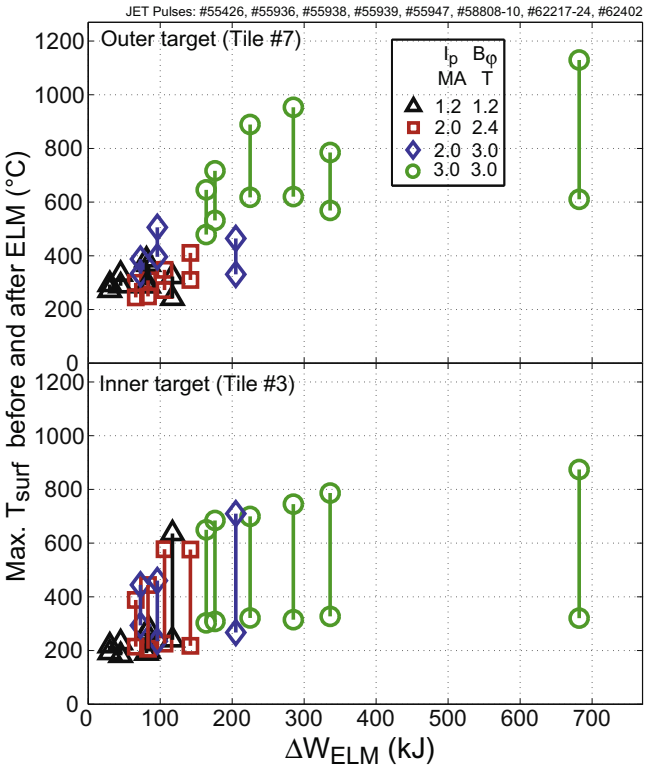

Fig. 5. Peak divertor T_{surf} before and during ELMs. Results are obtained from coherent averaging of ELM groups near the end of the H-mode phase.

The strong radiation asymmetry in favour of the inner divertor, which can reach as much as 5:1 (see [8]) is strongly suggestive that the deposited layers play a key role, especially since peak temperatures at the outer target are even higher than those observed at the inner (Fig. 5).

Whilst it cannot be proven with the available data, the impurity release is likely a combination of layer thermal decomposition and ablation. The former is known to be operative in the JET inner divertor, having been deduced from spectroscopic measurements of strong C_2 and CD emission in ELMing H-mode discharges with strike points positioned on the horizontal base tiles (numbers 4 and 6 in Fig. 1) where soft a-C:H layers are formed by redeposition of carbon eroded from the vertical tiles [11]. Such a process is also offered in [12] as an explanation for the non-linear increase in the erosion measured in JET beyond a given ELM size using in situ quartz micro balance detectors (the inner divertor QMB may be seen in Fig. 1). A possible explanation for the enhanced radiation seen at the highest ΔW_{ELM} in Fig. 4 is layer ablation, perhaps accompanied by the release of macroscopic clusters. Both thermal

decomposition and ablation provide a rich source of carbon which would radiate strongly depending on the efficiency with which the released particles penetrate the inner divertor plasma, itself changing rapidly on the timescale of the transient.

Energy densities on the JET inner vertical target during the rise phase of the ELM pulse at the highest ΔW_{ELM} in these experiments are ~0.15 MJ m^{-2}, around a factor of 3 below the values thought to be tolerable at the ITER targets before material damage under repetitive thermal loading occurs [1]. Evidence presented here for enhanced impurity release on large ELM impact at the inner target on JET demonstrates that disintegration of co-deposited layers on ITER is a very real possibility even for small ELMs (a 1 MJ ELM on ITER, corresponding to ~0.5 MJ m^{-2} target energy density, represents only 0.3% of W_{plasma}). This phenomenon is expected to be a major source of dust evolution in ITER, with associated safety concerns. In the case of both CFC and W targets, the co-deposits are expected to be dominated by Be evolved from the main chamber [13] so that the likely behaviour under impulsive energy loads cannot be directly extrapolated from the these JET results.

4. Main wall energy loads

Now seen in all tokamaks where they have been sought [14] and on a variety of diagnostics at JET [15–18], ELM filaments convecting plasma rapidly across the magnetic field in the scrape-off layer (SOL) to main chamber surfaces are a potential concern for ITER. A recent addition to the JET diagnostic set is a wide angle, main chamber viewing IR camera system which supplies some hitherto inaccessible data concerning first wall power loads [19]. Inspection of the IR images obtained in the relatively low triangularity discharges discussed here, reveals essentially no ELM interaction with the upper dump plates and none on the inner wall. By far the largest deposition occurs on the divertor targets, but there is a non-negligible interaction with the low field side bumper limiters, of which there are 16 on JET of roughly similar design extending ~50° poloidally above and below the outer mid-plane and separated approximately equally in the toroidal direction.

In all but one of the discharges in the series described here, the camera was employed in full frame mode, viewing the full poloidal cross-section with 4.2 ms time resolution, by far insufficient to resolve the time variation of the ELM energy deposition. Estimating a toroidal temperature profile (poloidally averaged) for all times on each of the 15 tiles comprising a typical bumper limiter and subsequently computing power fluxes, yields the time variation of the accumulated energy per tile. Only in cases with relatively infrequent ELMs (such as pulse #70226 shown in Fig. 2) can individual ELM heat pulses be detected in the accumulated energy time traces. In this case, the energy deposited on the bumper limiter within the IR camera FOV due to the initial fast ELM crash can be obtained in the same way as for the radiated power increase due to ELMs (see Fig. 3(a)), namely by estimating the difference in energy before and after the initial impulse, even if the poor time resolution is insufficient to determine the detailed dynamics of the deposited power flux density during the ELM. Since many of the large ELMs are compound (Fig. 2), this procedure allows the energy deposition on the limiter during the compound phase to be crudely separated from that immediately following the first crash. For discharges with higher gas fuelling (pulses #70221-3 in Table 1), the ELM frequency is too high and the ELM amplitude too low for the individual events to be detected in the IR energy time trace. Since these ELMs are rarely followed by a compound phase, it suffices to sum the accumulated energy on all tiles at the end of the H-mode phase to obtain an estimate of the total energy deposited by the filaments. The total energies derived in this way nevertheless represent lower limits. In all cases, no energy is assumed to reach the limiters during inter-ELM phases and it is further assumed that all 16 limiters receive identical averaged heat fluxes.

Fig. 6 illustrates this process for the zero gas fuelling, large ELM discharge of Fig. 2, where the image slices to the right show the limiter in question in ambient IR (i.e. without plasma) and during a single ELM. In general, the strongest interaction occurs on tiles in the outside mid-plane vicinity (Tiles 11–13 in Fig. 6), reflecting the ELM filament power exhaust localisation (see also [18]). Temperature excursions on these tiles can be significant (Fig. 6(b)), and, whilst there is indeed little or no rise during the inter-ELM periods, it is clear that the activity during the compound phases can be responsible for conveying significant energy to the limiters. The total accumulated energy for the example in Fig. 6 amounts to ~1.5 MJ, but only ~0.4 MJ is deposited immediately after the initial stored energy crash. This should be compared with a total stored energy loss of $\sum\Delta W_{ELM} \sim 11.7$ MJ (Fig. 6(c)). Table 1 compiles the results of this analysis for all shots in the series for which main chamber IR data are available. Within the relatively high uncertainty inherent in the approximations made to derive the wall ELM loading, there is evidently no variation in wall energy load fractions with average ELM energy (last column in Table 1).

Table 1
Summary of ELM statistics for 6 pulses in the 3.0 MA gas scan. Note that pulses 70225,6 have $\Gamma_{gas} = 0$.

Pulse	No. ELMs	$\sum\Delta W_{ELM}$ (MJ)	$\sum E_{LIM}$ (MJ)	$\langle\Delta W_{ELM}\rangle$ (MJ)	$\sum E_{LIM}/\sum\Delta W_{ELM}$ (%)
70221	143	34.5	1.57	0.241	4.6
70222	97	28.1	1.01	0.290	3.6
70223	64	23.4	0.87	0.371	3.7
70224	16	8.34	0.34	0.521	4.1
70225	29	15.1	0.59	0.520	3.9
70226	20	11.7	0.37	0.587	3.2

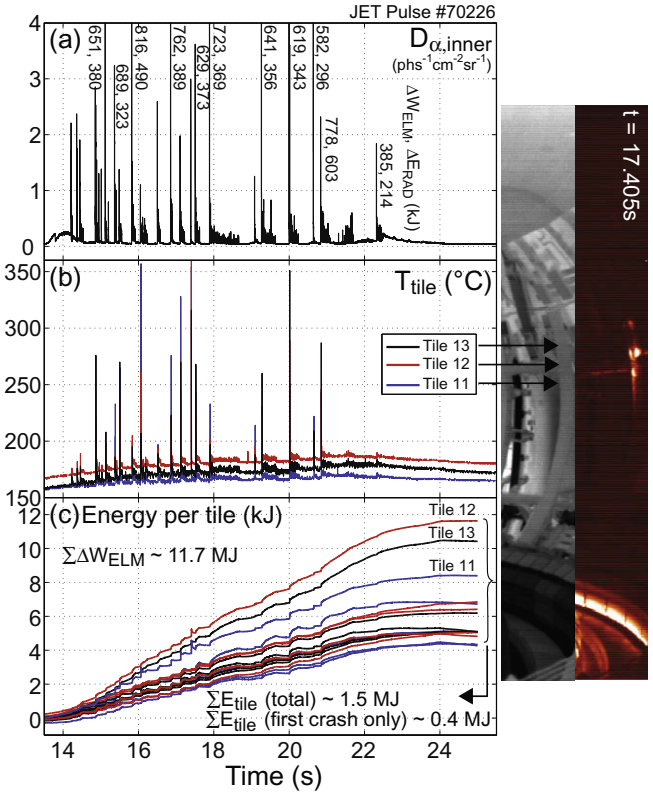

Fig. 6. Summary of ELM-wall energy deposition for the pulse of Fig. 2. Selected ELM peaks on the inner divertor D_α in (a) are marked with the corresponding ΔW_{ELM} and ΔE_{RAD}. (b) Peak T_{surf} on three tiles of a single outboard limiter. (c) Accumulated energy for all 15 tiles.

The ELM averaged wall loadings in Table 1 can be used to estimate average velocities for the ELM filament radial propagation by employing the parallel loss model that has been developed at JET [20] and successfully applied to a variety of experimental situations [15,20]. If pedestal plasma profiles are available, separatrix-wall gaps are known (fixed in all the discharges here at ~5 cm measured at the outer mid-plane) and an estimate for filament energy loss fraction is available, the model requires as input only a value for the cross-field ELM filament propagation speed, $v_{r,ELM}$ and an assumption for the point in space at which the filament originates [20]. Fig. 7(b) illustrates the application of the model to pulse #70224, for which good (pre-ELM) pedestal profiles of T_e and n_e are available (Fig. 7(a)) from the new JET High Resolution Thomson Scattering (HRTS) diagnostic. This is not, unfortunately, the case for the other discharges in the gas scan series. Based on these profiles, the pedestal width (shaded area in Fig. 7a) is ~4 cm, with $T_{e,pedt0} \sim 1500$ eV, $n_{e,pedt0} \sim 5 \times 10^{19}$ m^{-3} at the pedestal top, $T_{e,sep0} \sim 200$ eV, $n_{e,sep0} \sim 1 \times 10^{19}$ m^{-3} at the separatrix and $T_{e,pedm0} \sim 800$ eV, $n_{e,pedm0} \sim 3 \times 10^{19}$ m^{-3} at the mid-pedestal radius. The latter is a reference point often employed in the parallel loss model in the absence of any physics basis describing precisely where the ELM filaments originate [20].

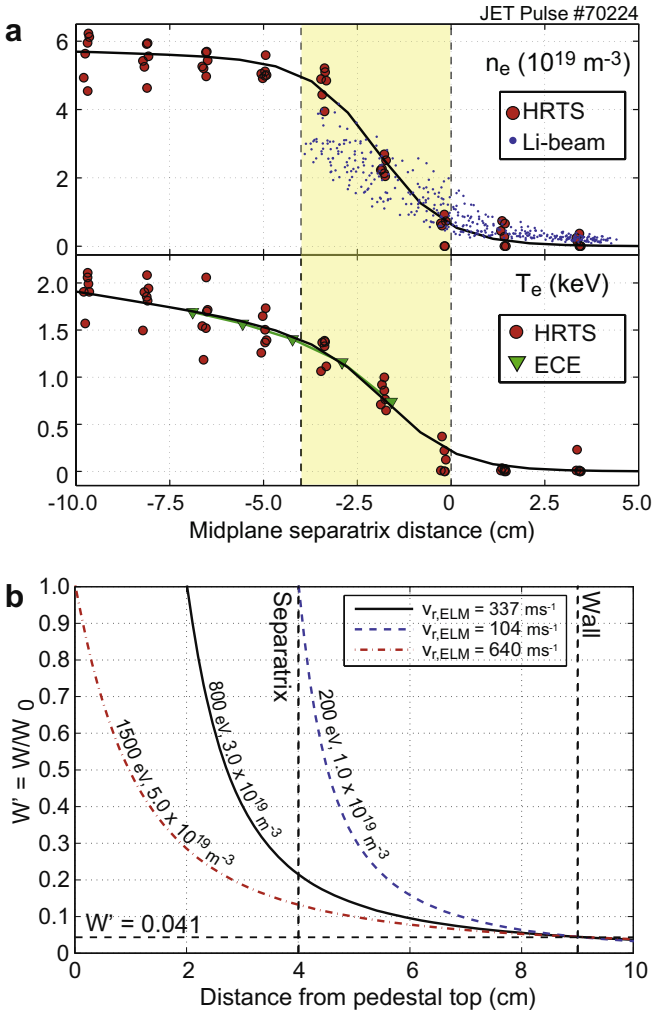

Fig. 7. (a) Inter-ELM pedestal profiles. Solid lines are tanh fits to the HRTS data. (b) Parallel loss model results for $W'(r)$ in ELM filaments with different origin (mid-pedestal, pedestal top and separatrix), but each depositing 4% of initial energy at the nominal limiter radius. Initial n_e,T_e at launch are marked.

For comparison with experiment, the parameter $W' = W/W_0$, the filament stored energy normalised to the initial value at the start of propagation is plotted in Fig. 7(b) for filaments originating at the pedestal top, the mid-pedestal radius and at the separatrix (assuming $T_i = T_e$). A different value of $v_{r,ELM}$ is required in each case to generate the experimentally observed average wall energy fraction of ~4% (Table 1). The required ELM filament speeds fall in the approximate range $v_{r,ELM} = 0.1$–0.65 km s^{-1}. For comparison, previous experimental values, deduced from measurements of time delays between D_α light and limiter Langmuir probe ion flux signals, found $v_{r,ELM}$ in the range 0.45–0.75 km s^{-1} for high power H-modes [21].

5. Conclusions

If material damage to the ITER divertor targets is to be avoided, the maximum loss in plasma stored energy per ELM must be restricted to $\Delta W_{ELM} \sim 1$ MJ. Such values can already be approached in JET (e.g. $\Delta W_{ELM} \sim 0.9$ MJ) at high current, high input power and with low or zero gas fuelling ($n_e \sim 0.4 n_{GW}$). In the divertor, the impact of large ELMs on JET provokes intense radiation losses, mostly confined to the inner divertor volume, with average magnitude $\Delta E_{RAD} \sim 0.5 \Delta W_{ELM}$, for $\Delta W_{ELM} < 0.55$ MJ. For higher ΔW_{ELM}, greater fractional radiation losses occur, reaching ~$0.7 \Delta W$ELM at $\Delta W_{ELM} \sim 0.9$ MJ and indicating enhanced impurity release. The plasma Z_{eff} does not appear to be unduly perturbed by the ELM-induced impurity release. Peak divertor target surface temperatures are far short of the requirements for carbon sublimation, even at the highest ΔW_{ELM}, suggesting that thermal decomposition and ablation of co-deposited carbon layers on the inner target may be occurring.

On average, ELMs are found to deposit between 3–4.5% of ΔW_{ELM} on main wall limiters, independently of average ELM energy. A model of ELM filament parallel energy losses developed at JET, when applied to the data for a specific discharge with large ELMs, requires radial ELM velocities in the range 0.1–0.65 km s^{-1} to explain the observed wall energy fractions, in reasonable agreement with previous measurements of these velocities on JET.

Acknowledgements

This work was conducted under the European Fusion Development Agreement and was supported in part by the Swiss National Science Foundation, EURATOM and the UK Engineering and Physical Sciences Research Council.

References

[1] A. Loarte et al., in: 22nd IAEA Fusion Energy Conference, 13–18 October 2008, Geneva, Switzerland, paper IT/P6-13.
[2] A. Loarte et al., Phys. Plasmas 11 (2004) 2668.
[3] R.A. Pitts et al., J. Nucl. Mater. 337–339 (2005) 146.
[4] A. Huber et al., J. Nucl. Mater. 363–365 (2007) 365.
[5] J.C. Fuchs et al., J. Nucl. Mater. 337–339 (2005) 756.
[6] T. Eich et al., J. Nucl. Mater. 363–365 (2007) 989.
[7] J.P. Coad et al., Nucl. Fus. 46 (2006) 350.
[8] A. Huber et al., J. Nucl. Mater. 390–391 (2009) 830.
[9] A. Loarte et al., Phys. Scr. T128 (2007) 222.
[10] W. Eckstein, V. Philipps, in: W. Hofer, J. Roth (Eds.), Physical Processes of the Interaction of Fusion Plasmas with Solids, Academic Press, San Diego, 1996.
[11] S. Brezinsek et al., J. Nucl. Mater. 337–339 (2005) 1058.
[12] A. Kreter et al., J. Nucl. Mater. 390–391 (2009) 38.
[13] J. Roth et al., these Proceedings, paper I-1.
[14] A. Kirk et al., J. Nucl. Mater. 390–391 (2009) 727.
[15] R.A. Pitts et al., Nucl. Fus. 46 (2006) 82.
[16] A. Alonso et al., J. Nucl. Mater. 390–391 (2009) 797.
[17] C. Silva et al., J. Nucl. Mater. 390–391 (2009) 355.
[18] M. Jakubowski et al., J. Nucl. Mater. 390–391 (2009) 781.
[19] E. Gauthier et al., J. Nucl. Mater. 363–365 (2007) 1026.
[20] W. Fundamenski, R.A. Pitts, Plasma Phys. Control. Fus. 48 (2006) 109.
[21] W. Fundamenski, W. Sailer, Plasma Phys. Control. Fus. 46 (2004) 233.